ACS OMEGA

http://pubs.acs.org/journal/acsodf

Article

Kinetics and Combustion Behavior of Atomized Zn−Mg Alloy Powder

Ming-xing Zhang, Chen-guang Zhu,* Xiao Xie, and Si-yu Liu

Cite This: *ACS Omega* 2023, 8, 24503−24512

Read Online

ACCESS | Metrics & More | Article Recommendations

ABSTRACT: Using pyrolants instead of warhead charges can release red light and thick smoke for target practice to highlight the safety of the impact point and dud disposal. In order to find the ideal material, the combustion and kinetic properties of two Zn−Mg alloys at critical proportions were investigated. Thermogravimetry/differential scanning calorimetry (TG/DSC) experiments in pure oxygen were conducted with atomized Zn−Mg alloy powder in the ratio of 7:3 and the ratio of 8:2 with three particle diameters under different heating rates. The kinetic parameters of the six materials were obtained by ASTM E698 and Ozawa−Flynn−Wall (OFW) methods, indicating that the activation energy (E_α) of the 7:3 Zn−Mg alloy powder was lower than that of the 8:2 Zn−Mg alloy powder when the particle size distributions are similar. By the method of nonlinear multivariate regression, the oxidation reaction of Zn−Mg alloy powder was divided into two steps. The proportion of mass gain of the first-step reaction of 7:3 Zn−Mg alloy powder was 0.462−0.518, and the proportion of mass gain of the first-step reaction of 8:2 Zn−Mg alloy powder was 0.138−0.228. Reaction mechanism functions of the two-step reaction of Zn−Mg alloy oxidation were derived as $f(\alpha) = (1-\alpha)^n(1 + k_{cat}\cdot\alpha)$. The results of combustion experiments showed that the pyrolants composed of 7:3 alloy can burn stably to produce satisfactory smoke and light signals, while the pyrolants composed of 8:2 alloy cannot achieve this. The 7:3 Zn−Mg alloy powder is an ideal ingredient for pyrotechnic compositions.

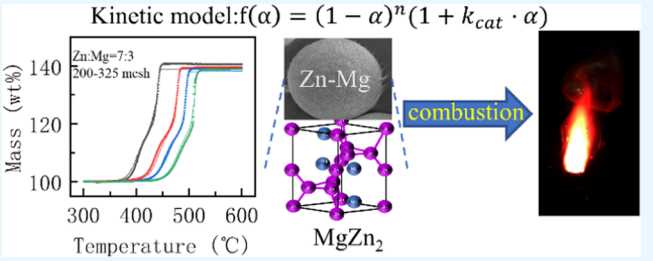

1. INTRODUCTION

Combat training is an essential mission in peacetime, but every year, there are casualties in the processing of shooting and misfire removal.[1−8] These needs prompted us to develop a new kind of pyrotechnic agent, which can produce light and smoke. It can show the explosive effect of the projectile before drilling into the ground, and there are no fragments within the whole process. In order to avoid killing debris and be unable to release it completely after entry into the ground, it is necessary for the pyrolant charge to be released immediately based on combustion mode rather than detonation. Therefore, critical materials that can produce deflagration are a priority.

Zinc (Zn) in its powder form has many applications in the pyrotechnic compositions. Pure zinc powder will emit intense white light when burning in pure oxygen, but it is difficult to burn in air. As an important pyrotechnic metal combustible agent, it has been combined with hexachloroethane or hexachlorobenzene to form a HC-type smoke agent.[9,10] The main components of the white smoke generated by combustion of Zn are ZnO and $ZnCl_2$. In recent years, since hexachloroethane or hexachlorobenzene has been restricted, the use of zinc in pyrotechnic materials has gradually decreased. However, due to the characteristics of low melting point and smoke performance, there is a certain demand for zinc powder in the formulation design of smoke agents and decoy agents. Some researchers[11,12] are trying to reuse it with high-energy oxidants, but there are indeed problems with difficult ignition and stable combustion. The typical examples are Zn/poly(tetrafluoroethylene) pyrotechnic compositions and $KMnO_4$/Zn pyrotechnic delay compositions.

Ordinary magnesium (Mg) powder has a particle size range of 10−100 μm, and its ignition point is roughly close to its melting point.[13,14] The average ignition temperature of magnesium powder (atomized spherical magnesium powder has a particle size of <45 μm and purity of 99.9%) is 719 K.[15] The maximum measured combustion temperature of Mg is about 3100 °C, which is very close to the magnesium adiabatic flame temperature in air, ca. 3200 °C.[16] As a volatile metal, it is easy to form a gas-phase diffusion flame with magnesium particles as the core, accompanied by dazzling white light. Magnesium powder is the most important combustible agent of pyrotechnics, which is easy to ignite. It is widely used in

Received: April 13, 2023
Accepted: June 5, 2023
Published: June 26, 2023

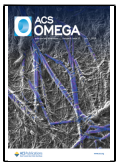

ACS Publications

© 2023 The Authors. Published by American Chemical Society

Table 1. Comparison of Physical and Chemical Properties of Magnesium and Zinc

	atomic weight	melting point, °C	boiling point, °C	density, g·cm^{-3}	calorific value		
					kJ·mol^{-1}	kJ·g^{-1}	kJ·cm^{-3}
Mg	24.3	648.9	1090	1.74	609.7	25	43.5
Zn	65.4	419	907	7.14	347	5.3	37.8

various pyrotechnic products after being mixed with an oxidizer in the powder form. Table 1 compares the properties of magnesium and zinc.[17,18]

Obviously, magnesium has many advantages. When the mass reaction enthalpy is compared, its advantages become more significant because the combustion efficiency is high. Compared with magnesium powder, zinc oxide produced by the combustion of zinc powder will block the continuous combustion of zinc particles, resulting in a relatively low energy release rate. Ignition difficulty is one of the main problems of zinc powder. Zhao et al.[19] studied the thermal and energetic behaviors of Mg−5% Zn and Mg−10% Zn alloys. They characterized the thermal behavior of Mg and Mg−Zn alloys at different heating rates of 10, 20, and 40 °C/min with DSC curves. They have calculated the apparent activation energy base on the first oxidization stage of Mg and Mg−Zn alloys. A remarkable decrease of apparent activation energy from ∼361.2 kJ/mol for Mg to ∼204.2−245.0 kJ/mol for Mg−Zn alloys is observed, which reveals that Zn and Mg−Zn intermetallic compounds could catalyze the oxidization of Mg. Zn−Mg alloy is expected to be an ideal combustible agent used in pyrolants, producing satisfactory smoke and light signals while having good reactivity. However, there are few studies on the kinetics and combustion behavior of Zn−Mg alloys.

Nine kinds of atomized spherical Zn−Mg alloy powder with the Zn/Mg mass ratios of 9:1, 8:2, 7:3, 6:4, 5:5, 4:6, 3:7, 2:8, and 1:9 were prepared. A series of experiments on the pyrotechnic formula were carried out; the Zn−Mg alloy powder was used as a combustible agent. The designed formulation was 10% NH_4ClO_4, 40% Zn−Mg alloy powder (200−325 mesh), 45% poly(vinyl chloride) (PVC), and 5% phenolic resin. Nitrocellulose strips were used for ignition. The formulations using Zn−Mg alloy powder with Zn/Mg mass ratios of 7:3, 6:4, 5:5, 4:6, 3:7, 2:8, and 1:9 could be ignited normally, while the formulations using Zn−Mg alloy powder with Zn/Mg mass ratios of 9:1 and 8:2 were difficult to ignite. Then, the formulation was successfully ignited using Zn−Mg alloy powder with a Zn/Mg mass ratio of 8:2, >325 mesh, as a combustible agent. It is considered that the 8:2 and 7:3 Zn−Mg alloy powders are in the critical position, in which pyrolants using 8:2 Zn−Mg alloy powder as a combustible agent is difficult to form a stable flame, while pyrolants composed of 7:3 Zn−Mg alloy powder can burn stably (see Section 3.4).

Since the middle of the 20th century, the equipment used in the measurement of thermal analysis (TA) and related data processing methods have developed rapidly to study reaction kinetics,[20,21] making thermal analysis one of the most common and widely used laboratory technologies.[22−25] Thermal analysis measurements include differential thermal analysis (DTA), differential scanning calorimetry (DSC), and thermogravimetry (TG).[26−30] Activation energy is the main potential factor for ignition and combustion of pyrotechnic materials.[31,32]

In the present work, the thermal oxidation process of atomized 8:2 and 7:3 Zn−Mg alloy powder with different particle sizes is studied by TG and DSC. Based on the ASTM E698 and Ozawa−Flynn−Wall (OFW) methods, the kinetic parameters, namely the activation energy and pre-exponential factor, are determined under non-isothermal conditions. By the method of nonlinear multivariate regression, kinetic models of atomized 8:2 and 7:3 Zn−Mg alloy powder are derived. The effect of Zn−Mg alloy as a combustible agent on the combustion of the pyrotechnic agent was analyzed by combustion experiments. The 7:3 Zn−Mg alloy powder and the 8:2 Zn−Mg alloy powder are indeed an obvious critical point for stable combustion by combustion experiments.

2. EXPERIMENTAL SECTION

2.1. Materials. The Zn−Mg alloy powder used in this paper was supplied by Tangshan Weihao Magnesium Powder Co., Ltd. The specific technical parameters of all the samples are shown in Table 2. The Zn−Mg powders had a spherical

Table 2. Specifications and Parameters of Six Samples

	D_{50} particle diameter, μm			
proportion of Zn−Mg alloy (wt %)	100−200 mesh	200−325 mesh	>325 mesh	energy contribution Zn:Mg
7:3 (Zn 65.8%)	93.09	61.44	34.48	29:71
8:2 (Zn 77.9%)	84.94	64.60	32.89	43:57

morphology (Figures 1a and 2a) with Zn and Mg uniformly distributed on the surface (Figures 1b−d and 2b−d). The XRD spectrum in Figure 1e shows that the main phases of 7:3 Zn−Mg alloy powder were Mg, $MgZn_2$, and $Mg_{102.08}Zn_{39.60}$. However, the compositions of the 8:2 Zn−Mg alloy powder were Mg and $MgZn_2$; the signal of $Mg_{102.08}Zn_{39.60}$ was not obvious (Figure 2e).

2.2. Instruments. The differential scanning calorimetry (DSC) tests were carried out using the management system of a Mettler-Toledo TGA/DSC3+ thermal analyzer made in Switzerland. Powder morphology was studied by field emission scanning electron microscopy (FESEM, JEOL JSM-7800F Prime). XRD (Bruker D8 Advance) was used to analyze the phase compositions of the samples. The combustion of the grains was recorded using a high-speed camera (FASTCAM Mini UX50).

2.3. Thermal Behavior Characterization. The thermal behaviors of the alloy powder in pure oxygen were determined based on differential scanning calorimetry (DSC) and thermogravimetric analysis (TG) experiments. During the test, the flow rate of oxygen was kept at 50 mL/min. Samples of about 2 mg were placed in Al_2O_3 pans with 70 μL volume. The experiments were performed at heating rates of 2, 5, 7, and 10 K/min from 100 to 800 °C. The choice of low heating rate was to better separate the exothermic peaks of the sample. The temperature calibration was conducted by heating In, Zn, Al, and Au through its melting transition. All experiments were performed twice to check the repeatability, which suggested good consistency by providing standard errors of ±1 °C.

https://doi.org/10.1021/acsomega.3c02496
ACS Omega 2023, 8, 24503−24512

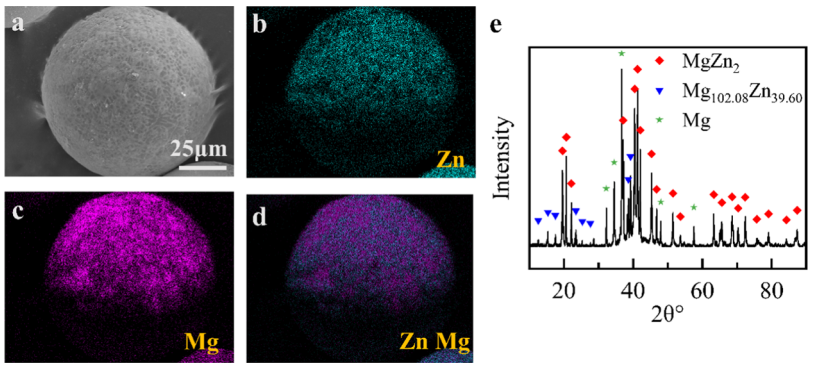

Figure 1. Zn−Mg (7:3) alloy powder characterized by SEM (a) and EDS (b−d) images and XRD spectrum (e). The XRD file numbers are Mg (PDF#35-0821), $MgZn_2$ (PDF#77-1177), and $Mg_{102.08}Zn_{39.60}$ (PDF#41-1292).

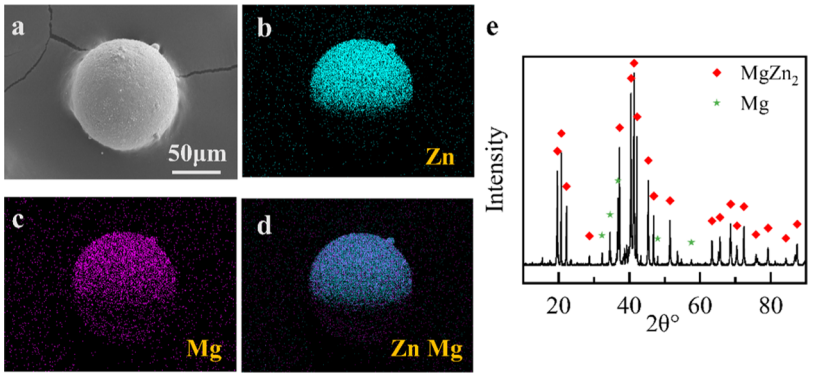

Figure 2. Zn−Mg (8:2) alloy powder characterized by SEM (a) and EDS (b−d) images and XRD spectrum (e). The XRD file numbers are Mg (PDF#35-0821) and $MgZn_2$ (PDF#77-1177).

2.4. Combustion Behavior Characterization. 1 g of the pyrolants was pressed into 6 mm-diameter grains with a pressure of 45 kg. The grains were ignited using nitrocellulose strips in an air environment. The combustion temperature of nitrocellulose strips is about 400 °C. The combustion of the grains was recorded using a high-speed camera (FASTCAM Mini UX50) at 250 frames/s.

3. RESULTS AND DISCUSSION

3.1. TG/DSC Curves of the Zn−Mg Alloy Powder in Pure Oxygen. The TG/DSC curves of the 7:3 and 8:2 Zn−Mg alloy powders in the mesh sizes of 100−200, 200−325, and >325 were measured at heating rates of 2, 5, 7, and 10 K/min in a pure oxygen atmosphere, which are shown in Figure 3.

Figure 3 shows the bimodal exothermic curves that may be related to separate combustion reactions of different alloy powders with oxygen. With the increase of the heating rate, the DSC curves of the Zn−Mg alloy powder gradually shift the direction of the temperature increase. All the characteristic temperatures including the onset temperature (T_e), peak temperature (T_p), and final temperature (T_f) are delayed; the results are shown in Tables 3 and 4. Meanwhile, as the heating rate increases, the exothermic curves become steeper, indicating that the exothermic reaction becomes more intense.[31,32]

By comparing the data of characteristic temperatures as shown in Tables 3 and 4 and combining with Figure 3, some obvious and complex differences can be found. First, there are two exothermic peaks in each DSC curve, and they separate almost under low heating rates, although the first exothermic peak of 8:2 Zn−Mg alloy powder is not obvious. Second, the T_e, T_p, and T_f of the 8:2 Zn−Mg alloy powder are higher than those of the 7:3 alloy powder under different heating rates and particle sizes, comparing Figure 3a vs Figure 3d, Figure 3b vs Figure 3e, and Figure 3c vs Figure 3f.

3.2. Calculation of the Kinetic Parameters of Thermal Decomposition in Pure Oxygen. The ASTM E698 and Ozawa−Flynn−Wall (OFW) methods[32] were used to determine the Arrhenius parameters for the thermal decomposition of Zn−Mg alloy powder (8:2) and Zn−Mg alloy powder (7:3). The ASTM E698 technique occupies an intermediate position between the model fitting and model-free methods. Determination of activation energies by ASTM methods requires a very accurate measurement of reaction peak temperatures (T_p) as a function of heating rates (β); the activation energy (E_α) and the pre-exponential factor (A) were calculated approximately from the following equations, respectively

$$E_\alpha = -2.19R\left[\frac{\mathrm{d}\lg(\beta)}{\mathrm{d}(1/T_p)}\right] \quad (1)$$

$$A = \frac{\beta E_\alpha}{RT_p^2}\exp\left(\frac{E_\alpha}{RT_p}\right) \quad (2)$$

where R is the gas constant and α is the conversion factor.

Figure 4 shows the plots of $\ln(\beta)$ against $1/T_p$ of Zn−Mg alloy powder under different mesh sizes. The activation energies of Zn−Mg alloy powder (8:2) and Zn−Mg alloy

https://doi.org/10.1021/acsomega.3c02496
ACS Omega 2023, 8, 24503−24512

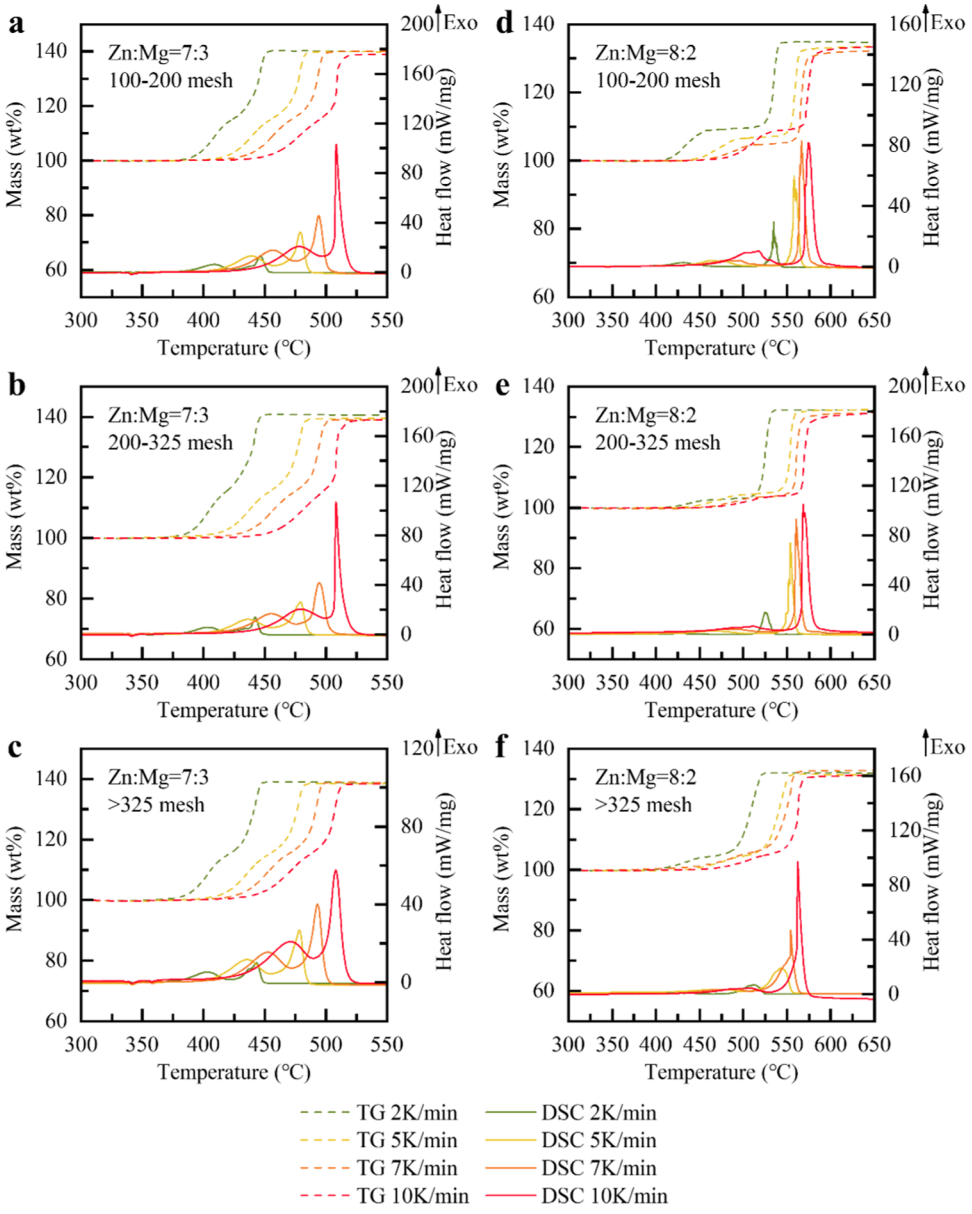

Figure 3. TG/DSC curves of 7:3 vs 8:2 Zn−Mg alloy powder with different particle diameters in pure oxygen. (a) 100−200 mesh 7:3 Zn−Mg alloy powder; (b) 200−325 mesh 7:3 Zn−Mg alloy powder; (c) >325 mesh 7:3 Zn−Mg alloy powder; (d) 100−200 mesh 8:2 Zn−Mg alloy powder; (e) 200−325 mesh 8:2 Zn−Mg alloy powder; and (f) >325 mesh 8:2 Zn−Mg alloy powder.

Table 3. Characteristic Temperatures of DSC Curves for Zn−Mg Alloy Powder (7:3) at Different Heating Rates

		the first peak			the second peak		
mesh size (mesh)	β (K/min)	T_e, °C	T_p, °C	T_f, °C	T_e, °C	T_p, °C	T_f, °C
100−200	2	370.4	408.8	424.8	424.8	446.4	459.7
	5	387.8	439.2	457.8	457.8	479.3	506.4
	7	402.8	457.0	475.0	475.0	494.1	517.7
	10	409.2	477.8	496.5	496.5	508.5	530.7
200−325	2	364.4	403.1	419.0	419.0	442.2	457.4
	5	386.1	436.2	455.9	455.9	479.4	498.5
	7	400.8	455.4	475.8	475.8	494.6	518.6
	10	408.3	479.2	499.8	499.8	508.3	530.8
>325	2	363.8	403.1	420.7	420.7	443.4	458.2
	5	384.0	435.8	454.9	454.9	478.2	496.0
	7	399.2	452.6	471.7	471.7	493.0	513.8
	10	410.0	471.2	489.2	489.2	508.0	531.5

https://doi.org/10.1021/acsomega.3c02496
ACS Omega 2023, 8, 24503−24512

Table 4. Characteristic Temperatures of DSC Curves for Zn−Mg Alloy Powder (8:2) at Different Heating Rates

		the first peak			the second peak		
mesh size (mesh)	β (K/min)	T_e, °C	T_p, °C	T_f, °C	T_e, °C	T_p, °C	T_f, °C
100−200	2	390.7	430.9	470.8	509.5	534.7	551.5
	5	425.4	463.4	499.3	538.8	558.0	585.8
	7	430.7	480.1	518.0	546.3	566.5	602.8
	10	435.8	517.7	545.5	551.7	574.8	609.2
200−325	2	397.5	429.0	467.8	505.5	525.0	539.1
	5	423.9	465.1	504.4	531.6	553.6	576.0
	7	433.1	493.2	521.7	537.9	560.4	598.1
	10	439.3	511.2	539.2	547.2	568.5	600.2
>325	2	380.7	418.1	462.1	467.7	512.8	527.2
	5	411.9	480.6	498.5	498.5	542.4	570.6
	7	416.1	490.3	508.1	508.1	554.1	577.6
	10	446.2	506.5	529.2	529.2	562.2	591.2

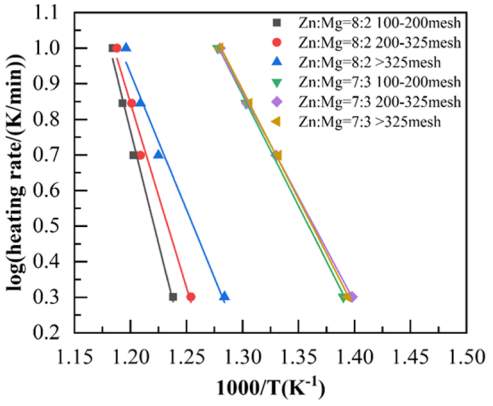

Figure 4. ASTM E698 fitting plots for thermal decomposition of Zn−Mg alloy powder at four heating rates.

powder (7:3) obtained from the slope of the fitting lines are shown in Table 5.

The OFW method[31−34] is a model-free method, which is developed independently by Ozawa, Flynn, and Wall. According to this method, eqs 3 and 4 are valid at different heating rates.

$$\log \beta = \log \frac{AE_\alpha}{RG(\alpha)} - 2.315 - 0.4567\frac{E_\alpha}{RT} \quad (3)$$

$$\log \beta = -0.4567\frac{E_\alpha}{R}\frac{1}{T} + C \quad (4)$$

Therefore, a plot of $\log\beta$ vs $1/T$ should yield a series of straight lines for different values of α taken at suitable regular intervals. The E_α values obtained by this method are independent of any mechanistic model. The variation trends of E_α and $\log A$, s^{-1} with different conversions (α) of Zn−Mg alloy powder are shown in Figure 5.

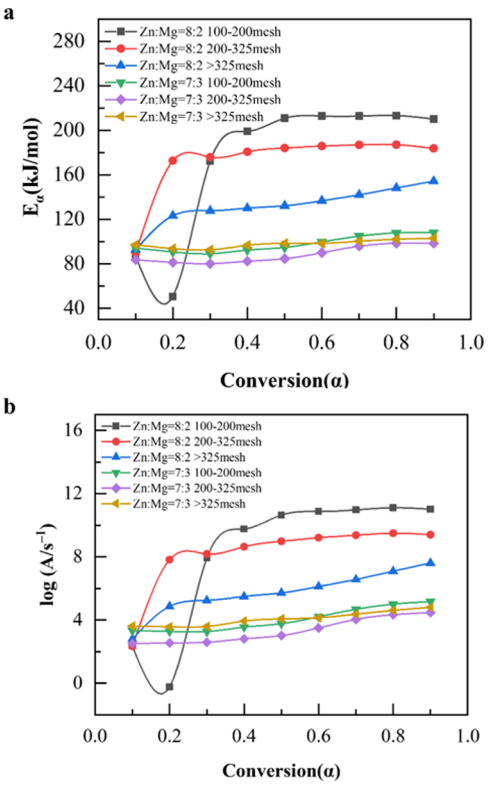

Figure 5. Variation of E_α (a) and $\log A$, s^{-1} (b) of Zn−Mg alloy powder with different mesh sizes depend on conversion (α = 0.1−0.9, with a 0.1 increase) calculated by the OFW method.

3.3. Determination of the Reaction Mechanism Function. It can be seen from Figure 3 that the oxidation of Zn−Mg alloy powder in oxygen is divided into two steps. The reaction mechanism function of these two steps was determined by a nonlinear multiple regression method. The

Table 5. Activation Energy (E_α) and Pre-exponential Factor ($\log A_\alpha$) of Zn−Mg Alloy Powder (7:3) and Zn−Mg Alloy Powder (8:2) Calculated by ASTM E698

	Zn−Mg alloy (7:3)			Zn−Mg alloy (8:2)		
mesh size (mesh)	E_α (kJ·mol^{-1})	deviation	$\log A$, s^{-1}	E_α (kJ·mol^{-1})	deviation	$\log A$, s^{-1}
100−200	108.50	±3.35	5.04	226.25	±15.00	11.64
200−325	101.05	±1.33	4.49	185.70	±15.97	9.07
>325	106.15	±1.64	4.94	133.07	±10.53	5.99

https://doi.org/10.1021/acsomega.3c02496
ACS Omega 2023, 8, 24503−24512

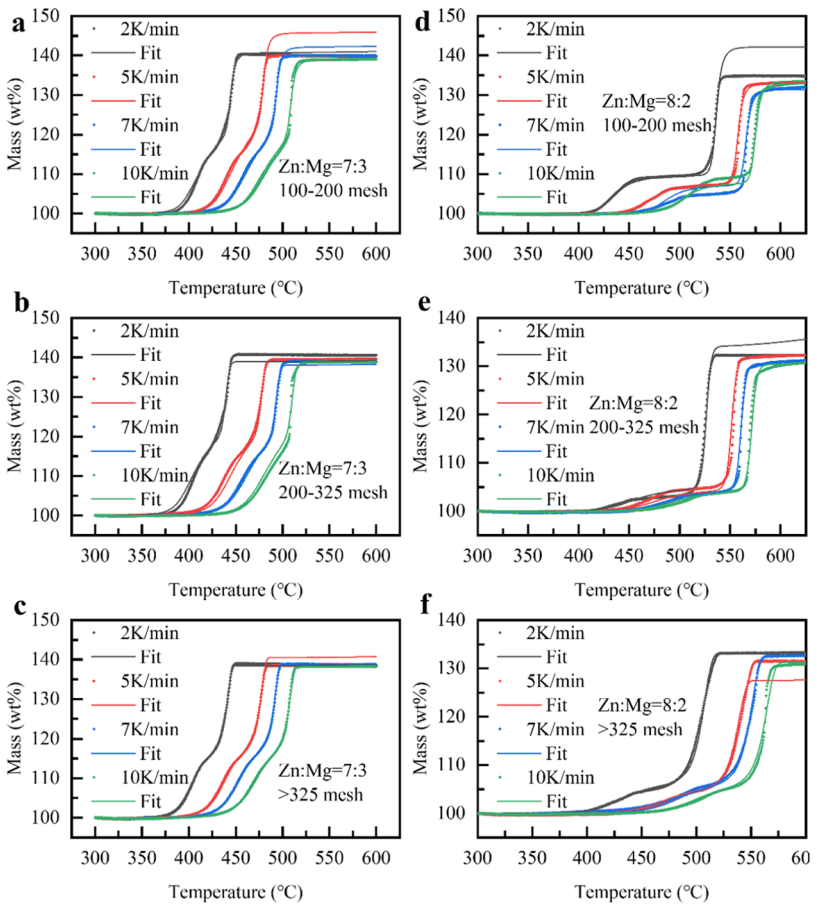

Figure 6. Comparison between experiments and simulation of TG curves for Zn−Mg alloy powder heating at 2, 5, 7, and 10 K·min^{-1}. (a) 100−200 mesh 7:3 Zn−Mg alloy powder; (b) 200−325 mesh 7:3 Zn−Mg alloy powder; (c) >325 mesh 7:3 Zn−Mg alloy powder; (d) 100−200 mesh 8:2 Zn−Mg alloy powder; (e) 200−325 mesh 8:2 Zn−Mg alloy powder; and (f) >325 mesh 8:2 Zn−Mg alloy powder.

Table 6. Optimum Values of Kinetic Parameters of Zn−Mg Alloy Powder by the Method of Nonlinear Multivariate Regression

	7:3 Zn−Mg alloy powder			8:2 Zn−Mg alloy powder		
kinetic parameters	100−200 mesh	200−325 mesh	>325 mesh	100−200 mesh	200−325 mesh	>325 mesh
$\log A_1$, s^{-1}	1.038	0.520	2.236	2.107	8.701	2.861
E_1 (kJ·mol^{-1})	85.15	72.85	90.52	97.14	169.96	94.63
reaction order 1 (n)	5.989	2.633	1.975	1.924	3.361	1.832
$\log K_{cat1}$	3.329	2.846	2.520	2.854	1.270	1.757
$\log A_2$, s^{-1}	2.803	2.242	2.572	7.626	4.465	5.675
E_2 (kJ·mol^{-1})	126.52	112.28	104.96	240.01	190.80	150.05
reaction order 2 (n)	1.402	0.948	0.660	1.515	1.113	0.753
$\log K_{cat2}$	5.153	4.266	3.109	6.117	6.265	2.161
proportion of reaction 1	0.507	0.518	0.462	0.228	0.138	0.178
correlation coefficient	0.9990	0.9988	0.9995	0.9979	0.9986	0.9984

TG curves simulated using software (NETZSCH thermo kinetics) and the experimental data are shown in Figure 6, and the optimum values of kinetic parameters are listed in Table 6. According to the fitting results, the reaction mechanism function for two steps conforms to the Cn model[35] (nth order with autocatalysis), $f(\alpha) = (1 - \alpha)^n (1 + k_{cat}\cdot\alpha)$, where n is the reaction order and k_{cat} is the autocatalytic kinetic rate constant.

It can be seen from Table 6 that the activation energies of the first-step oxidation reaction of Zn−Mg alloy powder are independent of the particle size, while the activation energies of the second-step oxidation reaction decrease with the decrease of the particle diameter. Similar to the view of Zhao et al.,[19] we believe that the melting of Zn−Mg intermetallic compounds and Zn occurs first during the heating process of the Zn−Mg alloy. As the temperature continues to rise, the oxidation of the alloy particle surface leads to the first stage of weight gain. Then, the self-propagating reaction and oxygen diffusion under the oxidation layer promote the rupture of the dense oxidation layer. The fragmented particles rapidly oxidize in contact with oxygen, resulting in the second stage of weight gain. Due to the presence of oxide shells on the surface of particles, the particle size has little effect on the oxidation of the alloy particle surface. However, when the oxide shell of particles is broken, the smaller the particle size, the smaller the generated fragments, and the oxidation process of alloy fragments

https://doi.org/10.1021/acsomega.3c02496
ACS Omega 2023, 8, 24503−24512

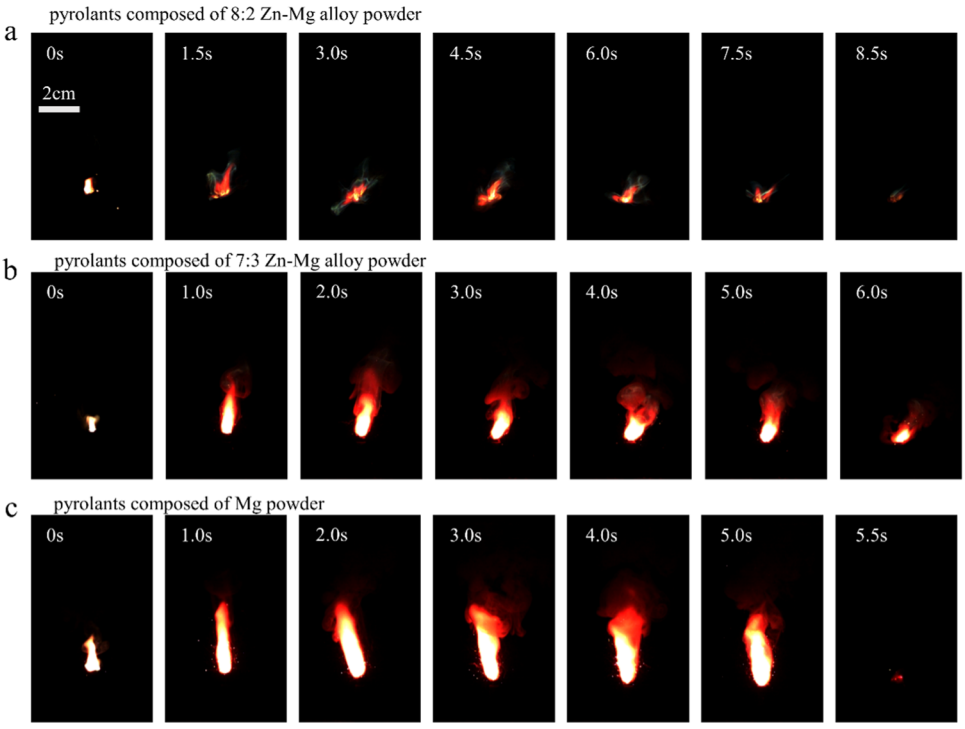

Figure 7. High-speed photography of pyrolants composed of (a) 8:2 Zn−Mg, (b) 7:3 Zn−Mg, and (c) Mg powder.

becomes faster. Therefore, the activation energies of the first step of Zn−Mg alloy oxidation are independent of its particle size, while the activation energies of the second-step decrease with the decrease of particle size.

The 7:3 Zn−Mg alloy powder has a higher proportion of mass gain (0.462−0.518) of the first-step reaction, while the 8:2 Zn−Mg alloy powder has a lower proportion of mass gain (0.138−0.228) of the first-step reaction, which leads to the activation energies of the 8:2 Zn−Mg alloy powder decrease with the decrease of particle size, and the activation energies of 7:3 Zn−Mg alloy powder are independent of the particle size. The values of the correlation coefficient are between 0.9979 and 0.9995, and the kinetic parameters are all within a reasonable range, indicating that the reaction mechanism function is reliable.

3.4. Crystal Analysis of the Zn−Mg Alloy Powder. The ratio of the intact $MgZn_2$ crystal is 65.4 × 2: 24.3≈84:16, which is close to 8:2 ratio obviously. Wang et al. used the first-principles calculation of density functional theory to analyze the electronic structure and related magnetic properties of the $MgZn_2$ phase.[36] They determined that the Zn−Mg bond is a polar covalent bond and that $MgZn_2$ is an alloy powder with a fairly stable spatial structure.[37] According to the literature,[38] $MgZn_2$ is the second stable crystal structure only to Mg_2Zn in the Zn−Mg alloy, which has a strong resistance to external force deformation and is a ductile material.[39]

According to the literature,[36,40] the Zn−Mg alloy powder with a complex crystal structure becomes liquid at 344°C, which is related to the zinc content.[41,42] When the Zn content varies from 0 to 4 wt %, it can be seen from the Mg−Zn phase diagram that when the Zn content exceeds 3 wt % at 893 K, it is likely to form a liquid phase.[43,44] With the further increase of the Zn content, the diffusion rate of Mg and Zn particles may be greatly increased due to the participation of the liquid phase. 344 °C is the temperature boundary point tending to form the liquid phase. With the increase of the Zn content, the pore diameter of the sintered compact decreases, as shown in Figures 1a and 2a. The first-step oxidation reaction is the surface oxidation of alloy particles, and the dense surface oxidation layer has hindered further oxidation to some extent. However, as the temperature continues to rise, the self-propagating reaction and oxygen diffusion under the oxidation layer promote the rupture of the dense oxidation layer and produce a strong exothermic reaction. The reaction intensity is the result of the complex action of the polycrystalline structure, and the reaction speed depends on the type and content of the composite crystal. The different pore diameters on the surface of the Zn−Mg alloy powder result in different proportions of the first-step reaction of the alloy. The proportion of the first-step reaction of 7:3 Zn−Mg alloy powder is 0.462−0.518, and the proportion of the first-step reaction of 8:2 Zn−Mg alloy powder is 0.138−0.228.

Therefore, for pyrotechnics, the Zn−Mg alloy (7:3) is more ignitable than the Zn−Mg (8:2) alloy, which can cause violent combustion. The activation energy ($E\alpha$) of the Zn−Mg alloy powder (7:3) is lower than that of the Zn−Mg alloy powder (8:2) under the same particle diameter range.

3.5. Combustion Rate Comparison and Charge Test. The pyrolants are produced, which can release light and smoke, and the pyrolants are based on the 8:2 Zn−Mg and 7:3 Zn−Mg alloy powder; in addition, the pure Mg powder is added for comparison. Three metal powders are the same in both the content and the particle size (200−325 mesh) in the pyrolants. The pyrolants are pressed into 6 mm-diameter grains with a pressure of 45 kg after being weighed and then ignited from one end. Figure 7 shows the combustion properties of pyrolants composed of 8:2 Zn−Mg alloy powder, 7:3 Zn−Mg alloy powder, and Mg powder by high-speed photography. As shown in Figure 7, the flame produced by the combustion of pyrolants composed of 8:2 Zn−Mg alloy powder is small and unstable, and the smoke and light signals are not as good as those of the 7:3 Zn−Mg alloy powder. The

https://doi.org/10.1021/acsomega.3c02496
ACS Omega 2023, 8, 24503−24512

flame area of pyrolants composed of 7:3 Zn−Mg alloy powder is slightly smaller than that of the Mg powder, but the pyrolants composed of the 7:3 Zn−Mg alloy powder still produce a stable smoke and light signals. Therefore, the 7:3 Zn−Mg alloy powder is an ideal material to generate strong smoke and light signals, while the 8:2 Zn−Mg alloy powder cannot achieve a satisfactory luminous effect. The masses of the grains were 1 g, and the lengths of the grains were 14 mm (the pyrolants are based on the 8:2 Zn−Mg), 15mm (the pyrolants are based on the 7:3 Zn−Mg), and 21 mm (the pyrolants are based on Mg). A high-speed camera was used to record the combustion of the grains and determine the duration of the combustion. The linear combustion rate and mass combustion rate of each grain were determined based on this. The measurement of the burning rate was repeated seven times in parallel, Table 7. The linear burning rate of pyrolants composed of the 7:3 Zn−Mg alloy powder is 31.6 percent faster than that of pyrolants composed of 8:2 Zn−Mg alloy powder, and the quality burning rate of pyrolants composed of the 7:3 Zn−Mg alloy powder is 22.8 percent faster than that of pyrolants composed of the 8:2 Zn−Mg alloy powder, which means that the 7:3 Zn−Mg alloy powder has higher chemical reaction activity compared with the 8:2 Zn−Mg alloy powder.

Table 7. Combustion Rate of Zn−Mg Alloy Powder (8:2) and Zn−Mg Alloy Powder (7:3)

combustion rate	Zn−Mg (8:2)	Zn−Mg (7:3)	Mg
linear rate, $mm \cdot s^{-1}$	1.630	2.145	4.410
quality rate, $g \cdot s^{-1}$	0.1164	0.1430	0.2100

The pyrolant based on the 7:3 Zn−Mg alloy (200−325 mesh) is used as the main charge, and 500 g of the pyrolant is pressed into a projectile. The projectile is shot using a high-speed camera during combustion, and the photo is given in Figure 8a.

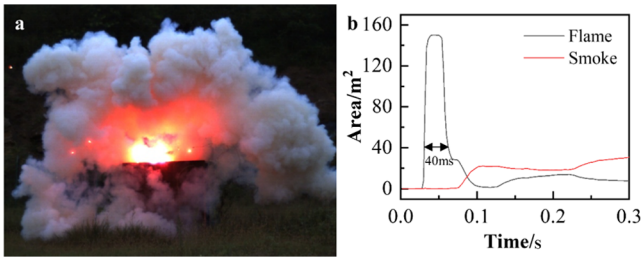

Figure 8. (a) High-speed photography of 500 g of the pyrolant. (b) Pyrotechnic charge forming light and smoke and its area curve.

Based on Figure 8b, it can be seen that the combustion release time is 40 ms. The main purpose of the development of Zn−Mg alloys was achieved by first showing flame and then gradually increasing smoke. Smoke and light interfere with each other, so the design uses a time difference, that is, light comes before smoke. The principle is that the combustion of the Zn−Mg alloy ensures the reaction speed while producing light, and then, the zinc reactant product absorbs water in the air to form smoke.

4. CONCLUSIONS

Oxidation reactions of the Zn−Mg alloy powder (7:3 and 8:2) in pure oxygen with different particle diameters of 100−200 mesh size, 200−325 mesh size, and >325 mesh size were studied using a simultaneous non-isothermal TG/DSC technique. The kinetic parameters of Zn−Mg alloy powder were obtained by ASTM E698 and Ozawa−Flynn−Wall (OFW) methods. The results indicate that the activation energy (E_α) of the Zn−Mg alloy powder (7:3) was lower than that of the Zn−Mg alloy powder (8:2) under the same particle diameter range. By the method of nonlinear multivariate regression, the two-step reaction of Zn−Mg alloy oxidation exhibited autocatalytic behavior, and the reaction mechanism function conformed to the Cn model (*n*th order with autocatalysis): $f(\alpha) = (1-\alpha)^n(1 + k_{cat}\cdot\alpha)$. The activation energies of the first-step oxidation reaction of Zn−Mg alloy powder were independent of the particle size, while the activation energies of the second-step reaction decreased with the decrease of the particle diameter. The proportion of the first-step reaction of 7:3 Zn−Mg alloy powder was 0.462−0.518, and the proportion of the first-step reaction of 8:2 Zn−Mg alloy powder was 0.138−0.228. Therefore, the activation energies of the 8:2 Zn−Mg alloy powder decrease with the decrease of particle size, and the activation energies of 7:3 Zn−Mg alloy powder are independent of the particle size. The combustion experiments showed that the pyrolants composed of 7:3 alloy can burn stably to produce satisfactory smoke and light signals, while the pyrolants composed of 8:2 alloy cannot achieve this. Although it is hoped that the alloy material contains more zinc to produce more smoke, based on the reaction speeds, the 7:3 Zn−Mg and the 8:2 Zn−Mg are indeed an obvious critical point in ignition and the complete reaction.

AUTHOR INFORMATION

Corresponding Author

Chen-guang Zhu − *School of Chemistry and Chemical Engineering, Nanjing University of Science and Technology, Nanjing 210094, P. R. China;* orcid.org/0000-0002-3549-0826; Email: zcg_lnkz@163.com

Authors

Ming-xing Zhang − *School of Chemistry and Chemical Engineering, Nanjing University of Science and Technology, Nanjing 210094, P. R. China*

Xiao Xie − *Science and Technology on Combustion and Explosion Laboratory, Xi'an Modern Chemistry Research Institute, Xi'an 710065, P. R. China*

Si-yu Liu − *Hunan Vanguard Group Co., Ltd., Hunan 410100, P. R. China*

Complete contact information is available at: https://pubs.acs.org/10.1021/acsomega.3c02496

Notes

The authors declare no competing financial interest.

ACKNOWLEDGMENTS

The work was supported by the National Natural Science Foundation of China (Project No. 51676100). The authors thank Tangshan Weihao Magnesium Powder Co., Ltd. for its support in the preparation of the zinc−magnesium alloy.

REFERENCES

(1) Kotwal, R. S.; Mazuchowski, E. L.; Stern, C. A.; Montgomery, H. R.; Janak, J. C.; Howard, J. T.; Butler, F. K.; Holcomb, J. B.; Eastridge, B. J.; Gurney, J. M.; Shackelford, S. A. A descriptive study of US

https://doi.org/10.1021/acsomega.3c02496
ACS Omega 2023, 8, 24503−24512

Special Operations Command fatalities, 2001 to 2018. *J. Trauma Acute Care Surg.* **2019**, *87*, 645−657.
(2) Patel, A. A.; Hauret, K. G.; Taylor, B. J.; Jones, B. H. Non-battle injuries among U.S. Army soldiers deployed to Afghanistan and Iraq, 2001-2013. *J. Saf. Res.* **2017**, *60*, 29−34.
(3) Darakjy, S.; Marin, R. E.; Knapik, J. J.; Jones, B. H. Injuries and illnesses among armor brigade soldiers during operational training. *Milit. Med.* **2006**, *171*, 1051−1056.
(4) Gong, P.; Mei, Z. G.; Liu, Z. C.; Yao, L. M.; Xiang, Y. Q.; Mei, C. In *Behavioral Errors Analysis and Research on Management and Control of Troops Training Based on REASON Model*, 16th International Conference on Man-Machine-Environment System Engineering (MMESE), October 21−23, 2016; pp 73−79.
(5) Park, T.-Y.; Yun, U. Causes and Lessons from USS John S McCain's Marine Accident. *Korean Assoc. Maritime Police Sci.* **2018**, *8*, 151−170.
(6) Namkung, S.-P. Developing the Safe Shooting Training System in Korea Reserve Forces: In Response to Gunfire Accidents. *Crisisonomy* **2016**, *12*, 97−107.
(7) Myjak, M. D.; Rosen, J. In *MEDNET: A Medical Simulation Network Grand Challenge*, Conference on Medicine Meets Virtual Reality, Newport Beach, CA, January 24−27, 2001; pp 341−347.
(8) Long, X.; Wang, X.; Zhou, P.; Xu, S.; Wang, Y.; Gui, L. Practice and reflection on practical training for tactical combat casualty care in military medical universities. *Milit. Med. Sci.* **2018**, *42*, 494−496.
(9) Jarvis, A. The combustion reactions of a pyrotechnic white smoke composition. *Combust. Flame* **1970**, *14*, 313−320.
(10) Karlsson, N.; Fangmark, I.; Haggqvist, I.; Karlsson, B.; Rittfeldt, L.; Marchner, H. Mutagenicity testing of condensates of smoke from titanium dioxide/hexachloroethane and zinc/hexachloroethane pyrotechnic mixtures. *Mutat. Res.* **1991**, *260*, 39−46.
(11) Panas, A. J.; Cudzilo, S.; Terpilowski, J. Investigation of the thermophysical properties of metal - polytetrafluoroethylene pyrotechnic compositions. *High Temp.−High Press.* **2002**, *34*, 691−698.
(12) Polis, M.; Szydlo, K.; Jarosz, T.; Procek, M.; Skora, P.; Stolarczyk, A. Investigation of Combustion of KMnO4/Zn Pyrotechnic Delay Composition. *Materials* **2022**, *15*, 18.
(13) Zhu, C. G.; Wang, H. Z.; Min, L. Ignition Temperature of Magnesium Powder and Pyrotechnic Composition. *J. Energ. Mater.* **2014**, *32*, 219−226.
(14) Shih, T. S.; Wang, J. H.; Chong, K. Z. Combustion of magnesium alloys in air. *Mater. Chem. Phys.* **2004**, *85*, 302−309.
(15) Ma, Y. S.; Zhang, K. C.; Ma, S. Z.; He, J. Y.; Gai, X. Q.; Zhang, X. G. Ignition and Combustion Characteristic of B center dot Mg Alloy Powders. *Materials* **2022**, *15*, 2717.
(16) Dreizin, E. L.; Berman, C. H.; Vicenzi, E. P. Condensed-phase modifications in magnesium particle combustion in air. *Combust. Flame* **2000**, *122*, 30−42.
(17) Dreizin, E. L. Effect of surface tension on the temperature of burning metal droplets. *Combust. Flame* **2014**, *161*, 3263−3266.
(18) Yuan, L.; Wang, C.; Cai, R. S.; Wang, Y. Q.; Zhou, G. W. Temperature-dependent growth mechanism and microstructure of ZnO nanostructures grown from the thermal oxidation of zinc. *J. Cryst. Growth* **2014**, *390*, 101−108.
(19) Zhao, W.; Jiao, Q.; Chen, P.; Yan, S.; Zhu, Y.; Zhang, B.; Zeng, X.; Liu, D.; Ou, Y.; Wang, F. Synergetic energetic kinetics of Mg-Zn alloys and pyrotechnics. *Combust. Flame* **2022**, *240*, No. 112000.
(20) Wang, S. Y.; Kossoy, A. A.; Yao, Y. D.; Chen, L. P.; Chen, W. H. Kinetics-based simulation approach to evaluate thermal hazards of benzaldehyde oxime by DSC tests. *Thermochim. Acta* **2017**, *655*, 319−325.
(21) Pouretedal, H. R.; Mousavi, S. L. Study of the ratio of fuel to oxidant on the kinetic of ignition reaction of Mg/Ba(NO3)(2) and Mg/Sr(NO3)(2) pyrotechnics by non-isothermal TG/DSC technique. *J. Therm. Anal. Calorim.* **2018**, *132*, 1307−1315.
(22) Dreizin, E. L.; Schoenitz, M. Correlating ignition mechanisms of aluminum-based reactive materials with thermoanalytical measurements. *Prog. Energy Combust. Sci.* **2015**, *50*, 81−105.
(23) Muravyev, N. V.; Monogarov, K. A.; Zhigach, A. N.; Kuskov, M. L.; Fomenkov, I. V.; Pivkina, A. N. Exploring enhanced reactivity of nanosized titanium toward oxidation. *Combust. Flame* **2018**, *191*, 109−115.
(24) Kök, M. V.; Varfolomeev, M. A.; Nurgaliev, D. K. TGA and DSC investigation of different clay mineral effects on the combustion behavior and kinetics of crude oil from Kazan region, Russia. *J. Pet. Sci. Eng.* **2021**, *200*, No. 108364.
(25) Kok, M. V.; Varfolomeev, M. A.; Nurgaliev, D. K. Low-temperature oxidation reactions of crude oils using TGA-DSC techniques. *J. Therm. Anal. Calorim.* **2020**, *141*, 775−781.
(26) Vlase, G.; Albu, P.; Doca, S. C.; Mateescu, M.; Vlase, T. The kinetic study of the thermally induced degradation and an evaluation of the drug−excipient interactions performed for a new-generation bisphosphonate-risedronate. *J. Therm. Anal. Calorim.* **2018**, *134*, 721−730.
(27) Wang, P.-c.; Qiang, X.; Yuangang, X.; Qiuhan, L.; Ming, L. A kinetic investigation of thermal decomposition of 1,1′-dihydroxy-5,5′-bitetrazole-based metal salts. *J. Therm. Anal. Calorim.* **2017**, *130*, 1213−1220.
(28) He, C. N.; Zhao, N. Q.; Han, Y. J.; Li, J. J.; Shi, C. S.; Du, X. W. Study of aluminum powder as transition metal catalyst carrier for CVD synthesis of carbon nanotubes. *Mater. Sci. Eng. A* **2006**, *441*, 266−270.
(29) Ravanbod, M.; Pouretedal, H. R.; Amini, M. K.; Ebadpour, R. Kinetic Study of the Thermal Decomposition of Potassium Chlorate Using the Non-isothermal TG/DSC Technique. *Cent. Eur. J. Energ. Mater.* **2016**, *13*, 505−525.
(30) Zhang, L.-k.; Zheng, X.-y. Experimental study on thermal decomposition kinetics of natural ageing AP/HTPB base bleed composite propellant. *Defence Technol.* **2018**, *14*, 422−425.
(31) Šesták, J. Ignoring heat inertia impairs accuracy of determination of activation energy in thermal analysis. *Int. J. Chem. Kinet.* **2019**, *51*, 74−80.
(32) Muravyev, N. V.; Pivkina, A. N.; Koga, N. Critical Appraisal of Kinetic Calculation Methods Applied to Overlapping Multistep Reactions. *Molecules* **2019**, *24*, 2298.
(33) Pouretedal, H. R.; Damiri, S.; Nosrati, P.; Ghaemi, E. F. The kinetic of mass loss of grades A and B of melted TNT by isothermal and non-isothermal gravimetric methods. *Defence Technol.* **2018**, *14*, 126−131.
(34) Singh, A.; Sharma, T. C.; Kumar, M.; Narang, J. K.; Kishore, P.; Srivastava, A. Thermal decomposition and kinetics of plastic bonded explosives based on mixture of HMX and TATB with polymer matrices. *Defence Technol.* **2017**, *13*, 22−32.
(35) Hong-Kun, Z.; Cao, T.; Dao-Sen, Z.; Wen-Lin, X.; Ya-Qong, W.; Qi-Shu, Q. Study on the non-isothermal kinetics of decomposition of 4Na(2)SO(4)center dot 2H(2)O(2)center dot NaCl. *J. Therm. Anal. Calorim.* **2007**, *89*, 531−536.
(36) Wang, H. M.; Zheng, R.; Li, G. R.; Li, P. S. First-Principles Research on the Electronic and Magnetic properties of MgZn2 Phase. *Chin. J. Inorg. Chem.* **2015**, *31*, 2143−2151.
(37) Wu, M. M.; Wen, L.; Tang, B. Y.; Peng, L. M.; Ding, W. J. First-principles study of elastic and electronic properties of MgZn2 and ScZn2 phases in Mg-Sc-Zn alloy. *J. Alloys Compd.* **2010**, *506*, 412−417.
(38) Zhou, D.-w.; Xu, S.-h.; Zhang, F.-q.; Peng, P.; Liu, J.-s. First-principle study on structural stability of Sn alloying MgZn2phase and Mg2Sn phase. *Chin. J. Nonferrous Met.* **2010**, *20*, 914−922.
(39) Hassan, S. F.; Siddiqui, O.; Ahmed, M. F.; Al Nawwah, A. I. Development of Gradient Concentrated Single-Phase Fine Mg-Zn Particles and Effect on Structure and Mechanical Properties. *J. Eng. Mater. Technol.* **2019**, *141*, No. 021007.
(40) Shuai, G.; Wu, Y. Q.; Shen, T.; Zhang, N.; Lai, L. S. Analysis of Zn-Mg Alloy Structure and Phases Distribution of Zn-Mg Diffusion System. *Acta Phys.-Chim. Sin.* **2012**, *28*, 2037−2043.
(41) Zhao, X. H.; Chen, C.; Chen, F. R. Effect of the precipitated phase of MgZn2 on surface nanocrystallization of Al-Zn-Mg alloy

https://doi.org/10.1021/acsomega.3c02496
ACS Omega 2023, 8, 24503−24512

based on high-frequency impacting and rolling. *Mater. Lett.* **2017**, *188*, 95−98.
(42) Liao, F.; Fan, S.; Deng, Y.; Zhang, J. First-principle Calculations of Mechanical Properties of Al2Cu, Al2CuMg and MgZn2Intermetallics in High Strength Aluminum Alloys. *J. Aeronautical Mater.* **2016**, *36*, 1−8.
(43) Liu, T.; Zhou, H.; Pan, F. *The Thermodynamics Calculation of Mg−Zn Alloy*; Trans Tech Publications Ltd.: Beijing, P. R. China, 2006; p 447.
(44) Jingyuan, Y.; Wang, J. Z.; Li, Q.; Shang, J.; Cao, J. M.; Sun, X. D. Effect of Zn on Microstructures and Properties of Mg-Zn Alloys Prepared by Powder Metallurgy Method. *Rare Met. Mater. Eng.* **2016**, *45*, 2757−2762.

https://doi.org/10.1021/acsomega.3c02496
ACS Omega 2023, 8, 24503−24512